Nature Methods

Principles for applying optogenetic tools derived from direct comparative analysis of microbial opsins

Joanna Mattis, Kay M Tye, Emily A Ferenczi, Charu Ramakrishnan, Daniel J O'Shea, Rohit Prakash, Lisa A Gunaydin, Minsuk Hyun, Lief E Fenno, Viviana Gradinaru, Ofer Yizhar & Karl Deisseroth

Supplementary Figure 1	Properties of depolarizing optogenetic tools
Supplementary Figure 2	Depolarizing tools: cell health, photocurrents, and temporal stationarity
Supplementary Figure 3	Comparison between cell-attached and whole-cell recordings of $ChR2_R$ and CatCh.
Supplementary Figure 4	Plateau potential
Supplementary Figure 5	Successful spikes and plateau potential for injected current-induced and light-induced depolarization
Supplementary Figure 6	Cell-type influences spiking response to electrical or optical depolarization
Supplementary Figure 7	Spike-timing and precision for depolarizing tools
Supplementary Figure 8	Properties of fast optogenetic tools
Supplementary Figure 9	$ChETA_A$ vs. $ChETA_{TR}$ spiking performance in acute slice: temporal stationarity, plateau, and spike success
Supplementary Figure 10	$ChETA_A$ vs. $ChETA_{TR}$ spike timing and precision: multiple spikes, latency, and latency spread across train
Supplementary Figure 11	$ChETA_A$ vs. ChIEF expression, cell health, and photocurrent stability
Supplementary Figure 12	$ChETA_A$ vs. ChIEF plateau potential, spiking performance and correlation with photocurrent
Supplementary Figure 13	$ChETA_A$ vs. ChIEF temporal stationarity, multiple spikes and correlation with photocurrent
Supplementary Figure 14	$ChETA_A$ vs. ChIEF spike latency and latency spread across a pulse train
Supplementary Figure 15	Hyperpolarizing tools: enhancement of membrane-trafficking and expression
Supplementary Figure 16	Properties of hyperpolarizing optogenetic tools
Supplementary Figure 17	Hyperpolarizing tool performance with prolonged stimulation
Supplementary Table 1	Naming convention for depolarizing optogenetic tools
Supplementary Table 2	Cloning and mutagenesis primers

Nature Methods: doi:10.1038/nmeth.1808

Supplementary Figure 1 Properties of depolarizing optogenetic tools

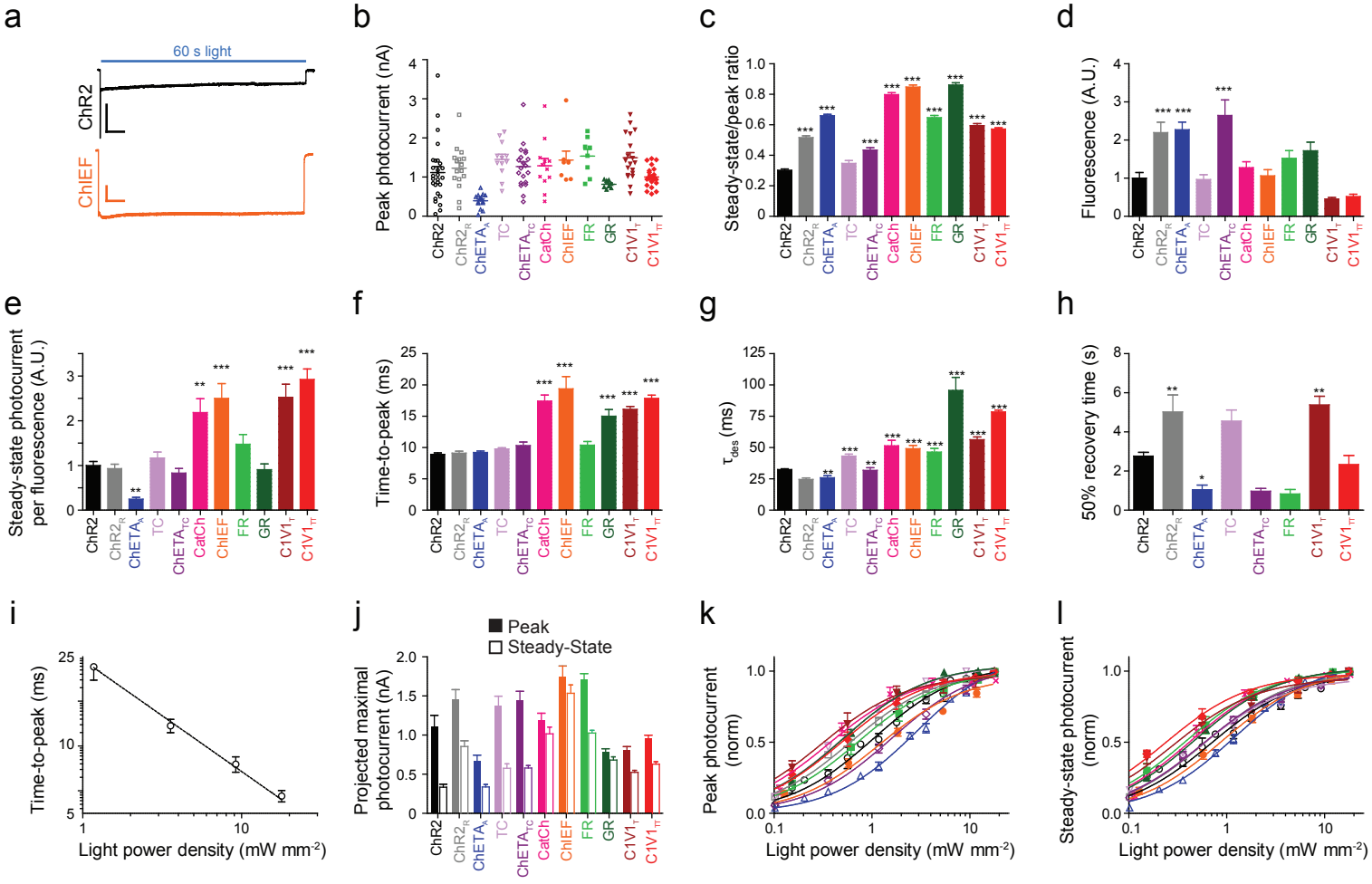

(**a**) Representative traces representing photocurrent response to 60 s continuous light (solid blue line) for ChR2 and ChIEF. Vertical and horizontal scale bars represent 500 pA and 5 s, respectively. (**b**) Spread of peak photocurrent around the mean for each depolarizing tool in response to a 1 s pulse of continuous light. Each colored dot represents an individual cell (*n* = 8-27). (**c**) Ratios of steady-state and peak photocurrents in response to a 1 s light pulse for all depolarizing tools (*n* = 8-54). (**d**) Normalized mean eYFP-fluorescence intensity (in arbitrary units, A.U.) measured from the soma of cells expressing depolarizing tools (*n* = 8-27). Values are normalized to ChR2 fluorescence. (**e**) Ratio of steady-state photocurrent to cell fluorescence intensity (*n* = 8-23). (**f**) Mean time-to-peak photocurrent in response to a 1 s light pulse for all depolarizing tools (*n* = 8-27). Note that time-to-peak is a photocurrent property (measured in voltage-clamp), in contrast with spike latency. (**g**) Mean desensitization kinetics (τ_{des}) for all depolarizing tools (*n* = 8-50). (**h**) Time required for 50% recovery from desensitization for all depolarizing tools (*n* = 5-20). (**i**) Time-to-peak photocurrent is significantly correlated with light intensity for ChR2 (R^2 = 0.74, *n* = 5). (**j**) Projected maximal peak and steady-state photocurrents (filled and hollow bars, respectively; *n* = 5-10). (**k**) Peak photocurrent for each cell is normalized to its maximum measured value and plotted against light power density (mW mm^{-2}; *n* = 5-10). Colors and shapes as in panel b. (**l**) Steady-state photocurrent for each cell is normalized to its maximum measured value and plotted against light power density (*n* = 5-15). Colors and shapes as in panel b. All population data is plotted as mean ± s.e.m. Stars indicate significance level: * $P < 0.05$, ** $P < 0.01$, *** $P < 0.001$. Unless otherwise indicated, $C1V1_T$ and $C1V1_{TT}$ were activated with 560 nm light, while all others were activated with 470 nm light, both at ~5 mW mm^{-2}.

Nature Methods: doi:10.1038/nmeth.1808

Supplementary Figure 2 Depolarizing tools: cell health, photocurrents and temporal stationarity

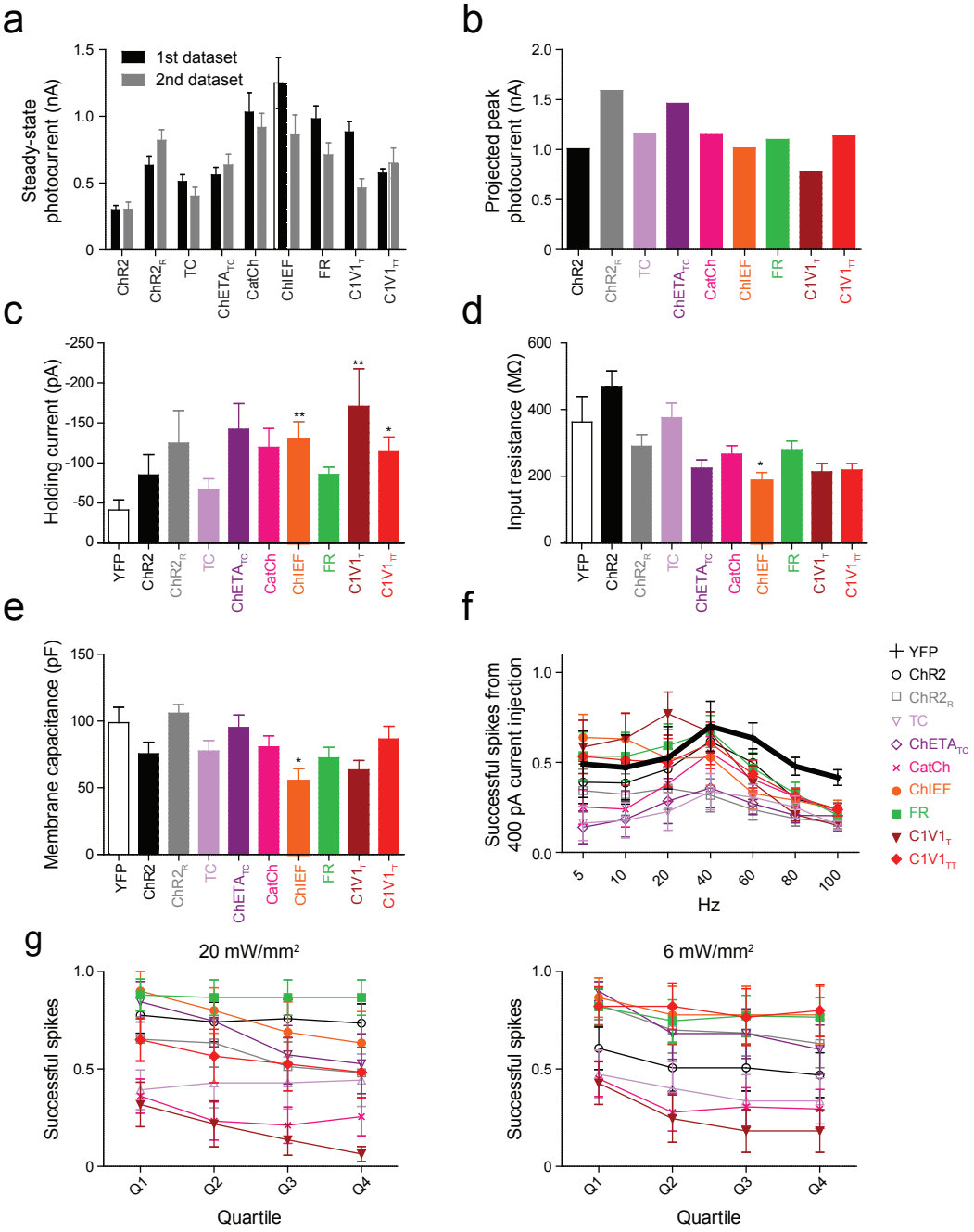

(**a**) The experiments for **Fig. 1** (main text) were performed at a different time to those for **Fig. 2** (main text), although all experimental conditions were matched. We confirmed that steady-state photocurrents from the two datasets were within a similar range (*n* for 1st dataset = 8-27, *n* for 2nd dataset = 7-18). (**b**) Peak photocurrents could not be directly measured from the cell-spiking experiments due to the presence of escape spikes in voltage-clamp. We therefore calculated the projected peak photocurrents from the steady-state photocurrents by using the steady-state/peak ratio as determined in **Fig. 1** of the main text. These values therefore have no error bars or associated statistics. (**c**) Current (pA) required to hold cells at -65 mV in voltage clamp for each tool, including eYFP control (white, hollow bar, *n* = 8-22). (**d**) Calculated input resistance (MΩ), including eYFP control (*n* = 8-23). (**e**) Calculated cell membrane capacitance (pF), including eYFP control (*n* = 8-20). (**f**) Proportion of successful spikes in response to injection of 400 pA current pulses (5 ms pulse width) at increasing frequency. eYFP control is plotted in black. (**g**) Temporal stationarity of depolarizing tools to 40 light pulses at 20 Hz at 20 mW mm^{-2} and 6 mW mm^{-2} (*n* = 9-18). A horizontal line indicates high temporal stationarity. All population data is plotted as mean ± s.e.m. Stars indicate significance level: * $P < 0.05$, ** $P < 0.01$, *** $P < 0.001$. $C1V1_T$ and $C1V1_{TT}$ were activated with 560 nm light, while all others were activated with 470 nm light.

Nature Methods: doi:10.1038/nmeth.1808

Supplementary Figure 3 Comparison between cell-attached and whole-cell recordings of $ChR2_R$ and CatCh

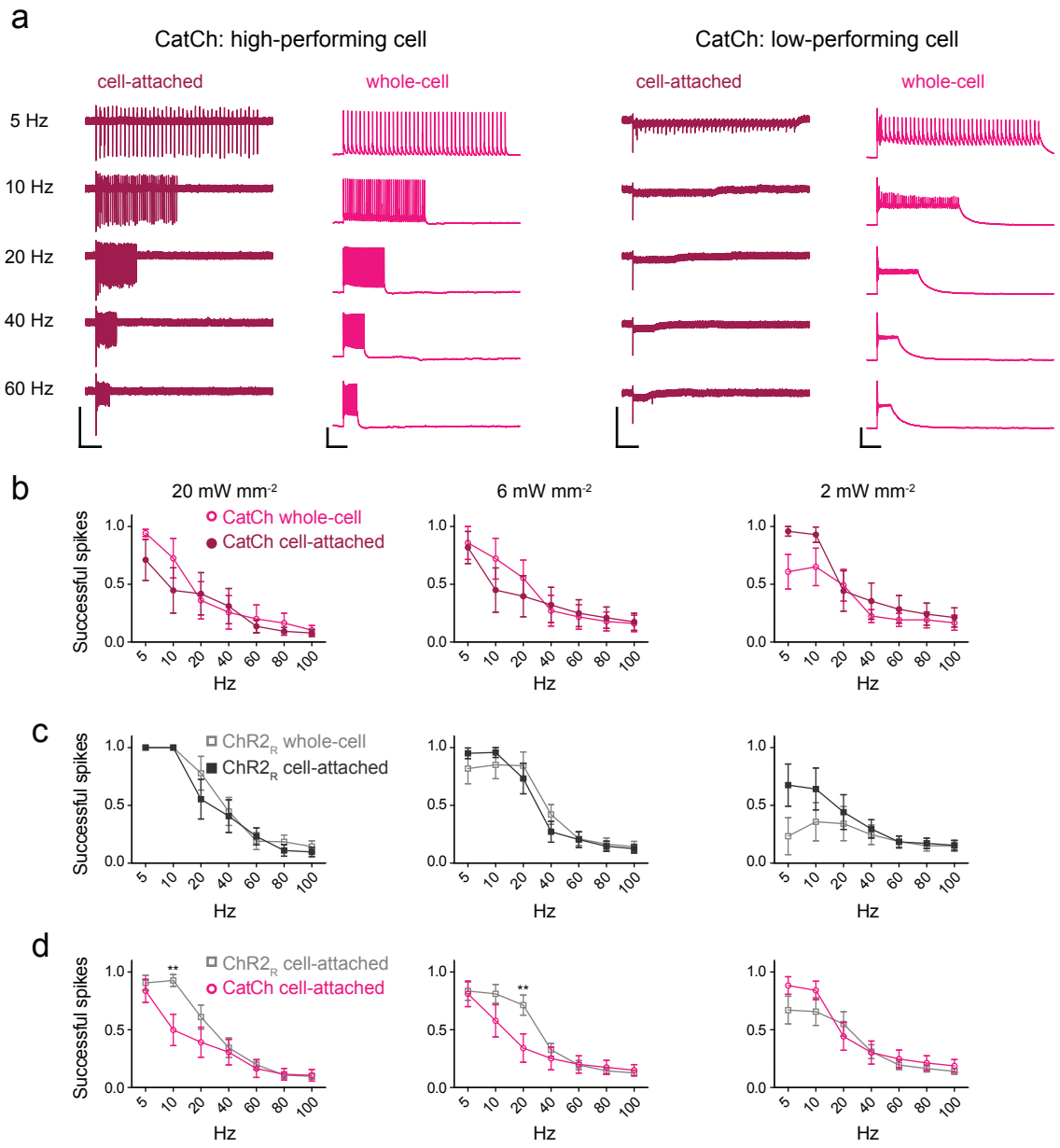

(**a**) Representative traces from two example cells expressing CatCh depicting spiking in cell-attached (voltage clamp) and whole-cell (current clamp) recordings. In each case, spikes were evoked by 40 light pulses (2 ms pulse-width), at increasing frequencies. Note the similarity in performance between cell-attached and whole-cell recording conditions in both cases. Vertical scale bars represent 40 pA or 40 mV for cell-attached (voltage-clamp) and whole-cell (current clamp) traces, respectively. Horizontal scale bars represent 1 s. (**b**) There is no significant difference in CatCh spiking performance between cell-attached (filled circle) and whole-cell (empty circle) recordings (n = 6-7). Proportion of successful spikes is plotted against stimulation frequency (5-100 Hz) at three different light intensities (20 mW mm^{-2}, 6 mW mm^{-2}, 2 mW mm^{-2}). (**c**) Similarly, there is no significant difference in $ChR2_R$ spiking performance between cell-attached (filled squares) and whole-cell (empty squares) recordings (n = 6-8). (**d**) Comparison of spiking performance between $ChR2_R$ (n = 15-19) and CatCh (n = 10-13) in cell-attached mode. ANOVA across all frequencies showed no overall difference between the two tools. However, on analysis of individual frequencies, $ChR2_R$ performed significantly better at 10 Hz under 20 mW mm^{-2} and at 20 Hz under 6 mW mm^{-2} ($P < 0.01$, Bonferroni post-tests). All population data is plotted as mean ± s.e.m. Stars indicate significance level: * $P < 0.05$, ** $P < 0.01$, *** $P < 0.001$. All cells were illuminated with 470 nm light.

Supplementary Figure 4 Plateau potential

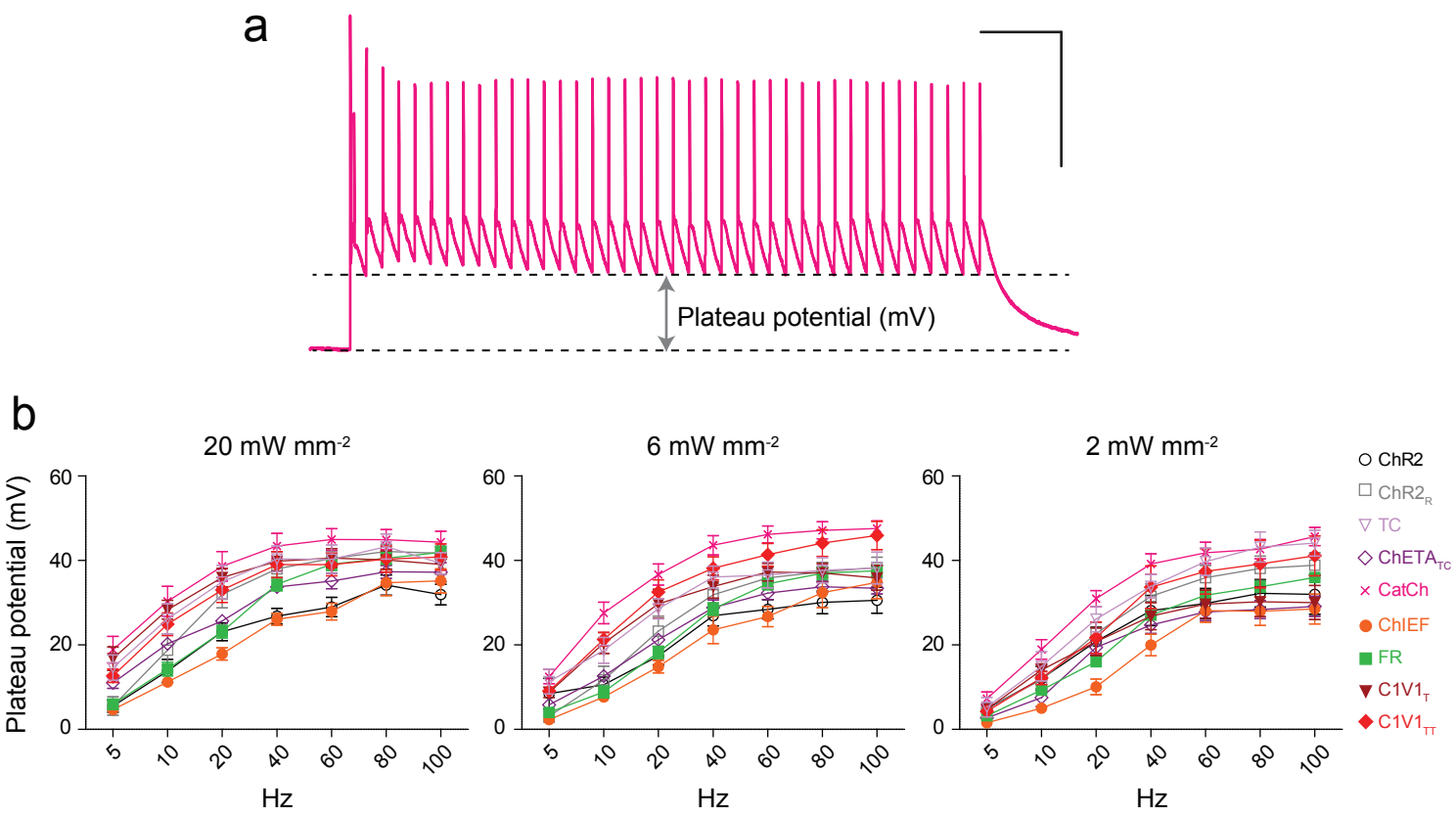

(**a**) Representative CatCh trace to illustrate measurement of plateau potential, the sustained depolarization concurrent with evoked spiking under current clamp. Vertical and horizontal scale bars represent 40 mV and 1 s, respectively. (**b**) Plateau potentials across stimulation frequencies at three different light intensities, 20 mW mm^{-2}, 6 mW mm^{-2} and 2 mW mm^{-2} (n = 5-17). At the highest light intensity, CatCh, TC and C1V1$_T$ had significantly larger plateau potentials compared to ChR2 at almost all frequencies. At the medium and lowest intensities, CatCh continued to have larger plateau potentials relative to ChR2 across the frequency range (p-value ranging from < 0.001 to < 0.05). All population data is plotted as mean ± s.e.m. Stars indicate significance level: * P < 0.05, ** P < 0.01, *** P < 0.001. C1V1$_T$ and C1V1$_{TT}$ were activated with 560 nm light, while all others were activated with 470 nm light.

Nature Methods: doi:10.1038/nmeth.1808

Supplementary Figure 5 Successful spikes and plateau potential for injected current-induced and light-induced depolarization

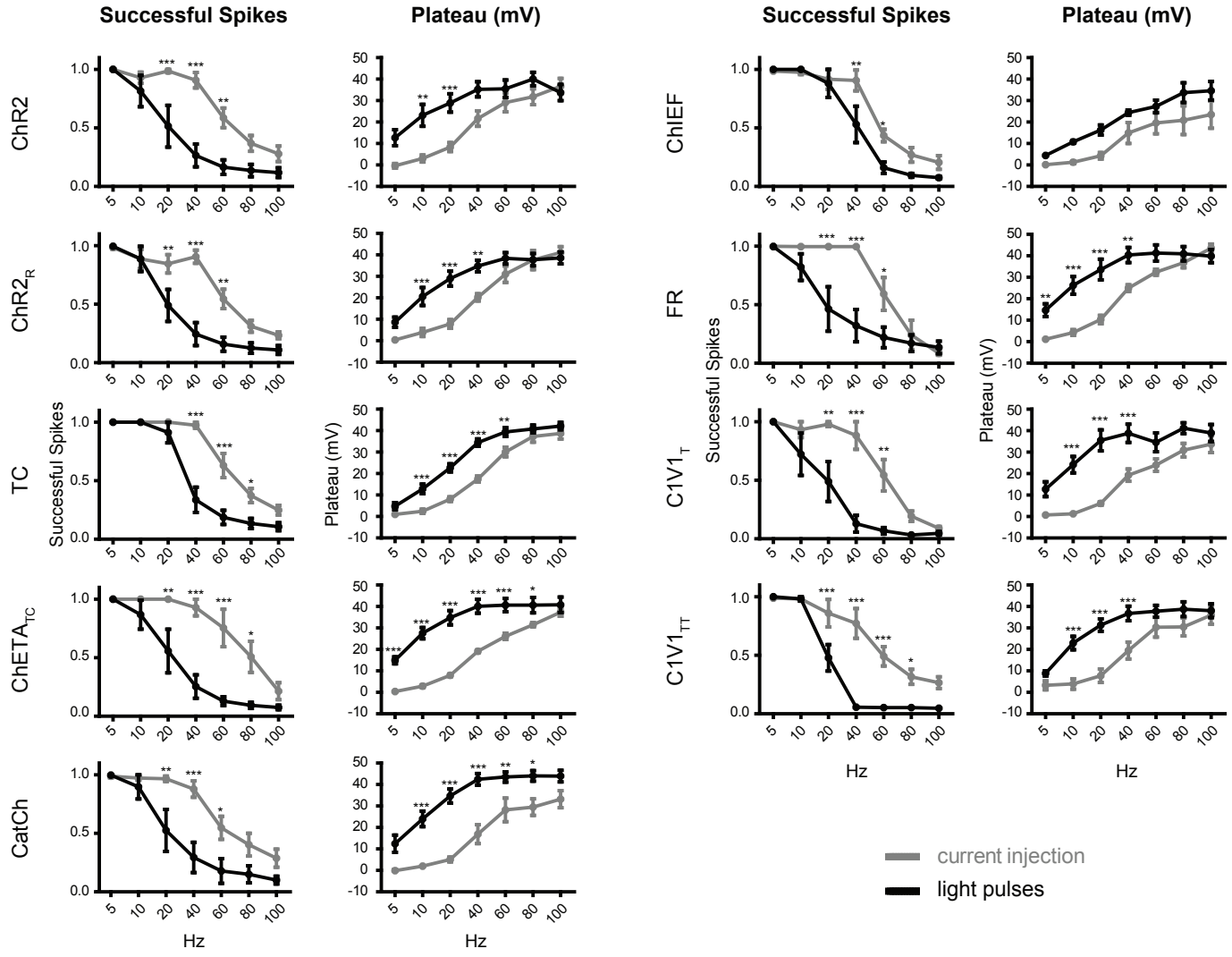

For each optogenetic tool, the left-side plot indicates proportion of successful spikes elicited by light and by supra-threshold current injection at increasing frequencies of stimulation (5 Hz to 100 Hz, 20 mW mm^{-2}; n = 5-11). The magnitude of the injected current was titrated for each cell in order to achieve high-fidelity spiking, and averaged from 500-700 pA for each group. Note that current injection curve is right-shifted relative to the light pulse curve, suggesting that current is more effective at eliciting spikes. These curves are closest for ChIEF, suggesting that, of the existing panel of excitatory tools, ChIEF represents the closest approach to current injection. The right-side plot shows increasing plateau potential with frequency of stimulation for current injection and light pulses. Note that plateau potential for light pulses is always greater than for current injection. In order to achieve a fair comparison between light pulses and current injection, we only included cells with greater than 90% successful spikes at 5 Hz. Stars indicate significance level for difference in spiking success between light pulses and current injection at individual frequencies (Bonferroni post-tests). All population data is plotted as mean ± s.e.m. Stars indicate significance level: * $P < 0.05$, ** $P < 0.01$, *** $P < 0.001$. $C1V1_T$ and $C1V1_{TT}$ were activated with 560 nm light, while all other tools were activated with 470 nm light.

Nature Methods: doi:10.1038/nmeth.1808

Supplementary Figure 6 Cell-type influences spiking response to optical or electrical depolarization

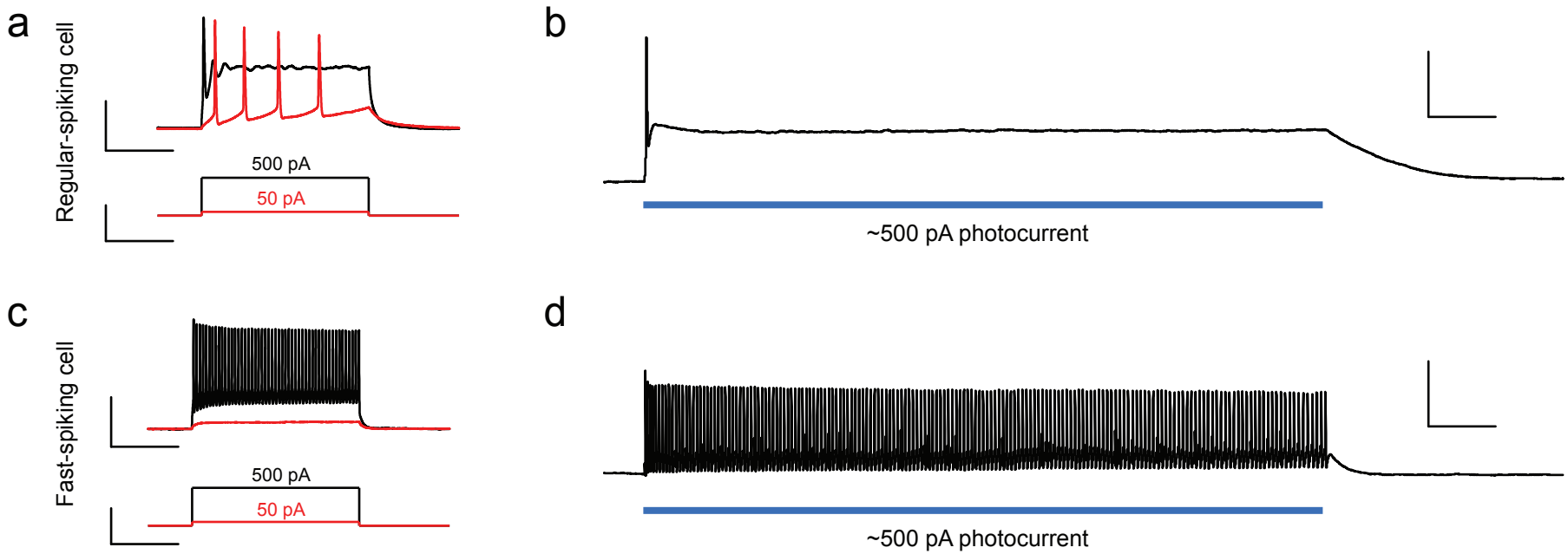

(**a**) Regular-spiking neuron: membrane potential response (in current clamp) to injection of current steps of 50 pA (red lower trace) or 500 pA (black upper trace). Depolarization by 50 pA elicits several spikes while 500 pA results in depolarization block and prevention of further spiking. Vertical scale bar represents 40 mV for voltage trace and 500 pA for current step trace; horizontal scale bar represents 100 ms. (**b**) Regular-spiking neuron: membrane potential response to 1 s of continuous blue light (indicated by the blue horizontal line below the voltage trace) for a cell expressing $ChR2_R$. This cell has a steady-state photocurrent of ~500 pA which, as for current injection, causes depolarization block and prevention of spiking. Vertical and horizontal scale bars represent 40 mV and 100 ms, respectively. (**c**) Fast-spiking neuron: membrane potential response (in current clamp) to injection of current steps of 50 pA (red lower trace) or 500 pA (black upper trace). In contrast to the regular-spiking neuron, 50 pA is insufficient to evoke spikes whereas 500 pA generates rapid firing with no evidence of adaptation or depolarization block. Vertical scale bar represents 40 mV for voltage trace and 500 pA for current step trace; horizontal scale bars represent 100 ms. (**d**) Fast-spiking neuron: membrane potential response to 1 s of continuous blue light for a cell expressing $ChETA_{TR}$. This cell has a similar steady-state photocurrent (~500 pA), which generates rapid and non-adapting spiking, as seen with current injection. Vertical and horizontal scale bars represent 40 mV and 100 ms, respectively. Cells were illuminated with 470 nm light at ~5 mW mm^{-2}.

Nature Methods: doi:10.1038/nmeth.1808

Supplementary Figure 7 Spike-timing and precision for depolarizing tools

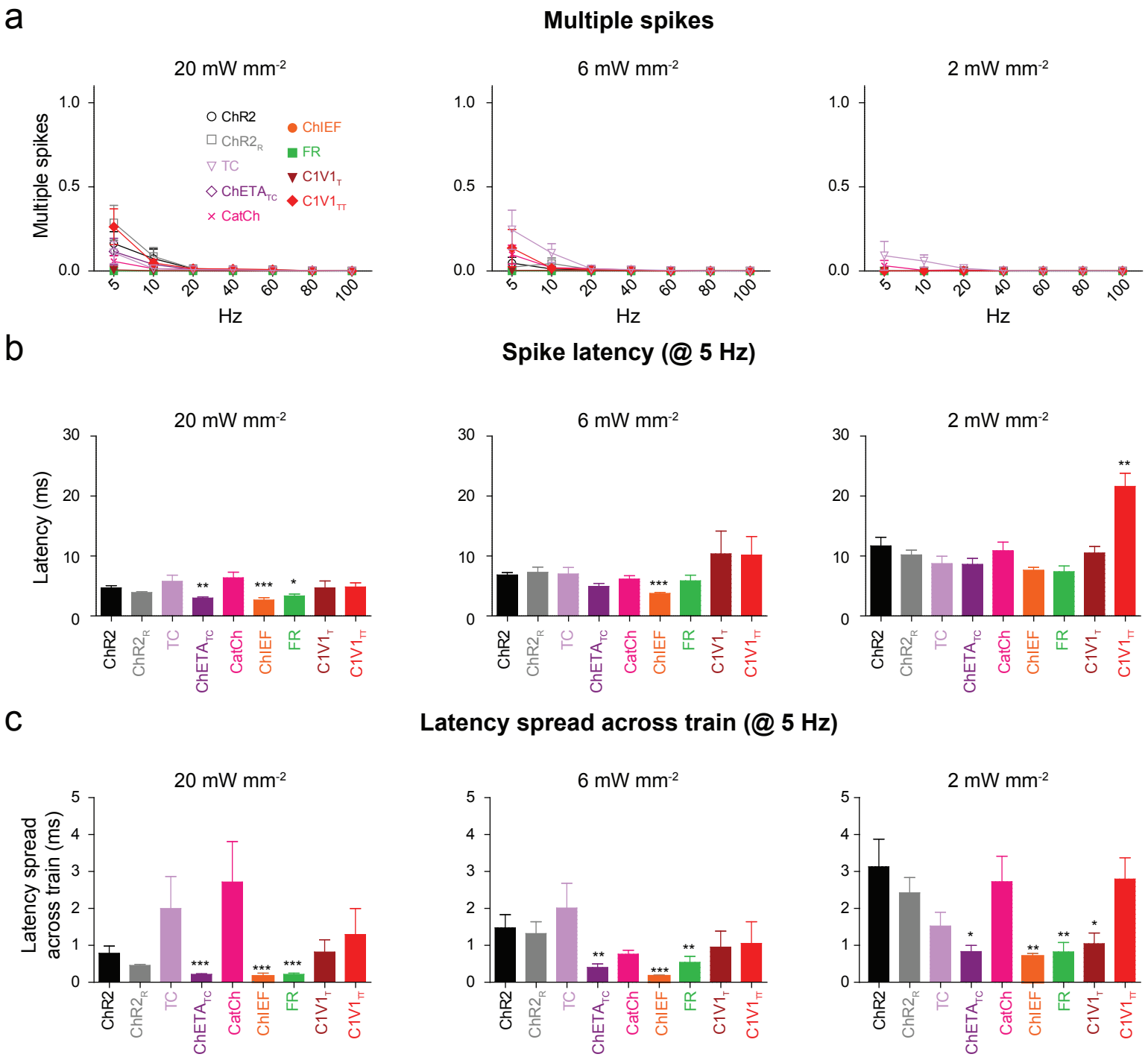

(**a**) Multiple spikes, defined as the proportion of light pulses (of a train of 40) eliciting more than one spike, plotted against frequency for three different light intensities: 20 mW mm^{-2}, 6 mW mm^{-2}, 2 mW mm^{-2} (n = 8-18). (**b**) Latency to spike at 5 Hz at three different light intensities: 20 mW mm^{-2}, 6 mW mm^{-2}, and 2 mW mm^{-2} (n = 4-16). (**c**) Latency spread across a 5 Hz pulse train for three different light intensities: 20 mW mm^{-2}, 6 mW mm^{-2}, 2 mW mm^{-2} (n = 4-16). All population data is plotted as mean ± s.e.m. Stars indicate significance level: * $P < 0.05$, ** $P < 0.01$, *** $P < 0.001$. C1V1$_T$ and C1V1$_{TT}$ were activated with 560 nm light, while all others were activated with 470 nm light.

Nature Methods: doi:10.1038/nmeth.1808

Supplementary Figure 8 Properties of fast optogenetic tools

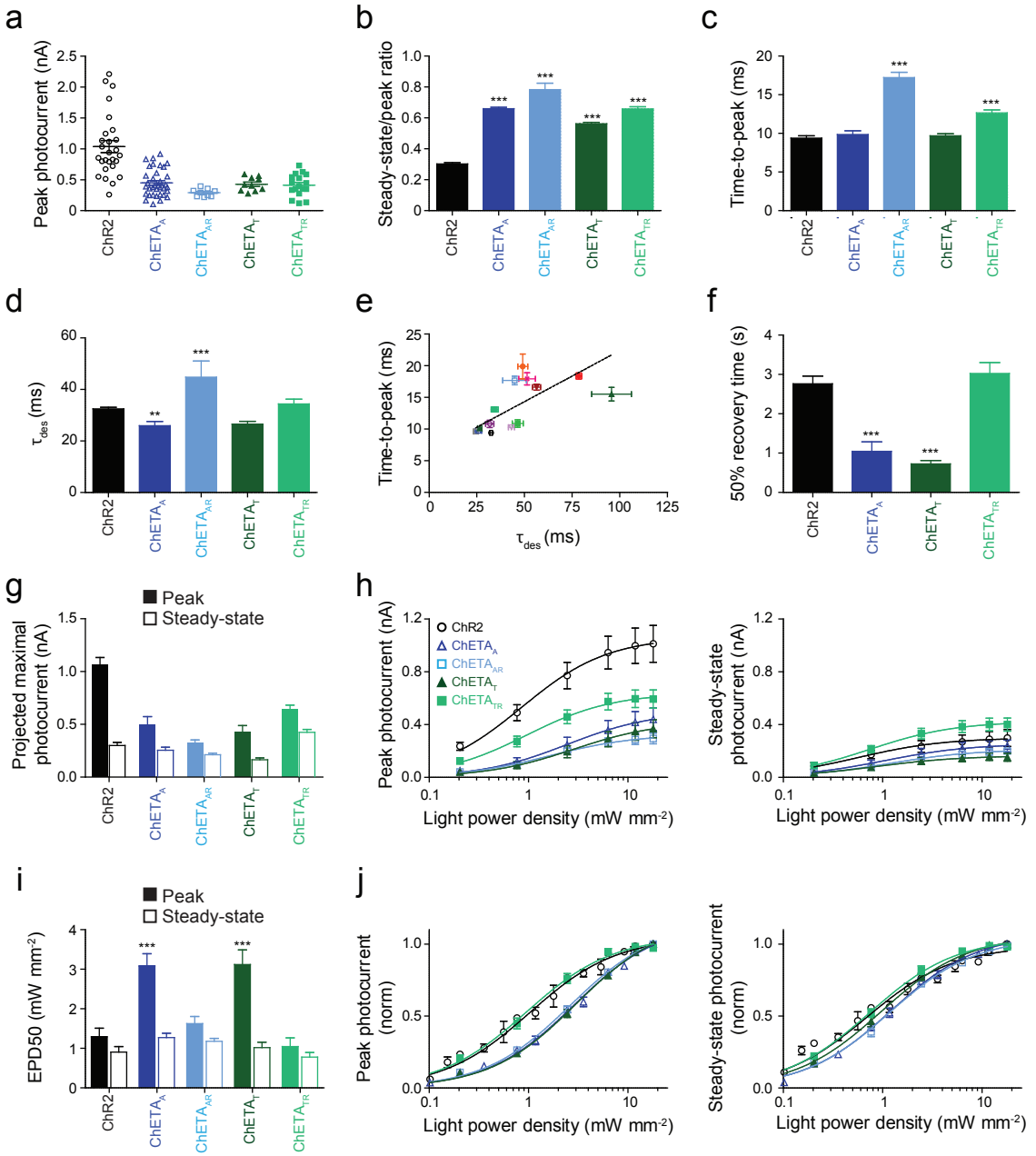

(**a**) Spread of peak photocurrent around the mean for each tool in response to a 1 s pulse of continuous light. Each colored dot represents an individual cell (n = 9-35). (**b**) Steady-state/peak ratios (n = 9-54). (**c**) Double mutants $ChETA_{AR}$ and $ChETA_{TR}$ take significantly longer to peak than ChR2 in response to a 1 s pulse of continuous light (n = 9-20). (**d**) Desensitization kinetics (τ_{des}) for ultra-fast optogenetic tools and ChR2 (n = 9-50). (**e**) Time-to-peak photocurrent vs. τ_{des}. $ChETA_T$, $ChETA_{TR}$, and $ChETA_{AR}$ are added to the same scatterplot shown in **Fig. 1f**. The black line represents the best fit regression. Color coding remains the same as for the main figures. (**f**) The single-mutant ChETAs recover more rapidly from desensitization than ChR2 (n = 8-20). $ChETA_{AR}$ was excluded from this analysis due to its high (> 75%) steady-state/peak ratio. (**g**) Projected maximal peak (filled bars) and steady-state (hollow bars) photocurrents based on the non-linear fit of raw peak photocurrent vs. light power (n = 5-15). (**h**) Peak and steady-state photocurrents across light power densities (n = 5-15). (**i**) $ChETA_A$ and $ChETA_T$, had significantly higher EPD50 for the peak relative to ChR2. In contrast, there were no significant differences in EPD50 for steady-state photocurrents (n = 5-15). (**j**) Normalized peak and steady-state photocurrents for each cell vs. light power density (mW mm^{-2}; n = 5-15). All population data is plotted as mean ± s.e.m.. Stars indicate significance level: * $P < 0.05$, ** $P < 0.01$, *** $P < 0.001$. All optogenetic tools were activated with 470 nm light, both at ~5 mW mm^{-2}.

Nature Methods: doi:10.1038/nmeth.1808

Supplementary Figure 9 ChETA$_A$ vs. ChETA$_{TR}$ spiking performance in acute slice: temporal stationarity, plateau, and spike success

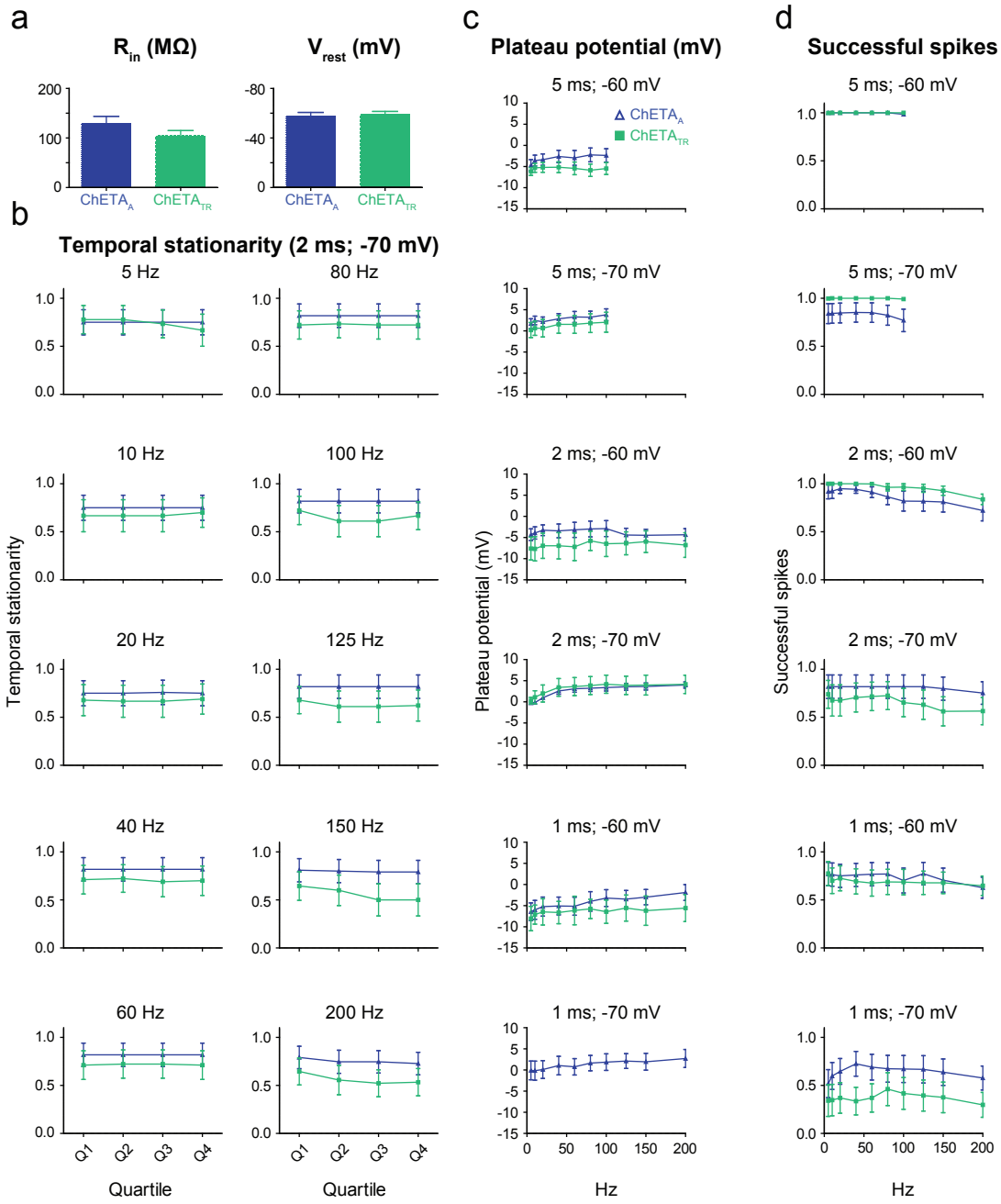

(**a**) Cell health comparison: input resistance (R_{in}) and resting membrane potential (V_{rest}) are similar for ChETA$_A$ (*n* = 19) and ChETA$_{TR}$ (*n* = 15). (**b**) Temporal stationarity across stimulation frequencies (5 Hz to 200 Hz, 2 ms pulse-width, -70 mV holding potential). The 40 pulses of the train are divided into quartiles and the proportion of successful spikes elicited in each quartile (out of 10) is quantified. ChETA$_A$ and ChETA$_{TR}$ show high temporal stationarity (horizontal lines) across the frequency range (*n* = 4-14 for ChETA$_A$; *n* = 9-10 for ChETA$_{TR}$). (**c**) Plateau potential vs. stimulation frequency (5-200 Hz for 1 and 2 ms pulse-width; 5-100 Hz for 5 ms pulse-width) across varying pulse-widths and holding potentials in current clamp. Panels from top to bottom represent 3 different pulse-widths (5 ms, 2 ms, 1 ms) and 2 different holding potentials (-60 mV, -70 mV). The plateau potential is negative as the spike waveform brings the membrane potential below baseline. The two optogenetic tools perform similarly across conditions (*n* = 4-14 for ChETA$_A$; *n* = 4-10 for ChETA$_{TR}$). The 1 ms/-70 mV condition is omitted for ChETA$_{TR}$ due to insufficient number of cells with sufficient spiking to calculate plateau. (**d**) Proportion of successful spikes vs. stimulation frequency (as above) across varying pulse-widths and holding potentials in current clamp. ChETA$_A$ and ChETA$_{TR}$ again perform similarly across conditions (*n* = 4-14 for ChETA$_A$; *n* = 9-10 for ChETA$_{TR}$). All population data is plotted as mean ± s.e.m. Stars indicate significance level: * $P < 0.05$, ** $P < 0.01$, *** $P < 0.001$. Cells were illuminated with 470 nm light at ~5 mW mm^{-2}.

Nature Methods: doi:10.1038/nmeth.1808

Supplementary Figure 10 ChETA$_A$ vs. ChETA$_{TR}$ spike-timing and precision: multiple spikes, latency and latency spread across train

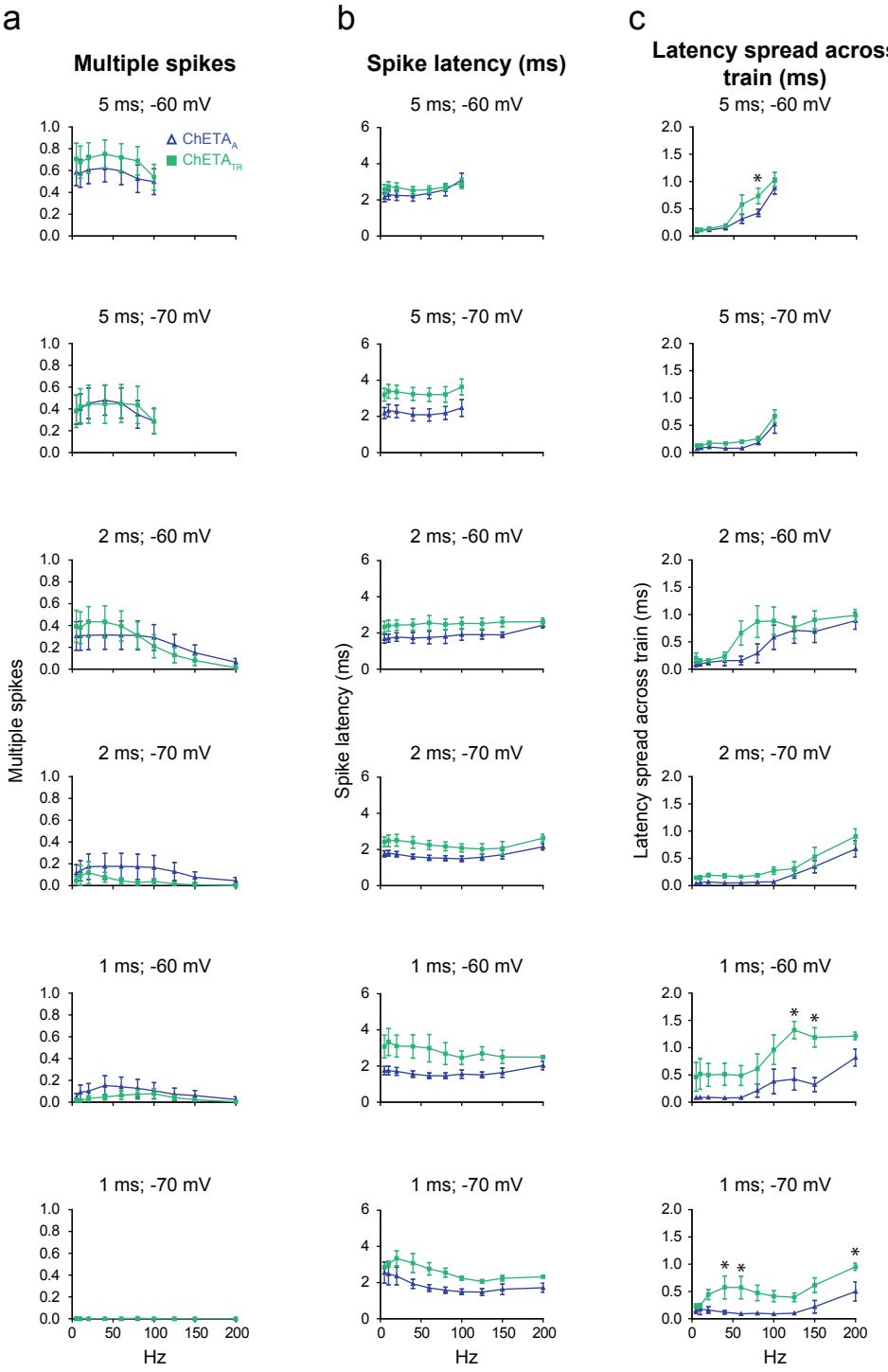

(**a**) Proportion of multiple spikes (light pulses eliciting more than 1 spike) vs. stimulation frequency (5-200 Hz for 1 and 2 ms pulse-width; 5-100 Hz for 5 ms pulse-width) across varying pulse-widths (5 ms, 2 ms, 1 ms) and holding potentials (-60 mV, -70 mV). ChETA$_A$ and ChETA$_{TR}$ perform similarly across conditions (n = 4-14 for ChETA$_A$; n = 9-10 for ChETA$_{TR}$). (**b**) Latency to spike vs. frequency across varying pulse-widths (5 ms, 2 ms, 1 ms) and holding potentials (-60 mV, -70 mV). ChETA$_A$ and ChETA$_{TR}$ perform similarly across conditions (n = 7-13 for ChETA$_A$; n = 3-10 for ChETA$_{TR}$). (**c**) Latency spread across train (standard deviation of spike latencies) vs. frequency across varying pulse-widths (5 ms, 2 ms, 1 ms) and holding potentials (-60 mV, -70 mV). ChETA$_A$ has significantly lower latency spread than ChETA$_{TR}$ in several conditions. n = 7-13 for ChETA$_A$; n = 3-10 for ChETA$_{TR}$. All population data is plotted as mean ± s.e.m. Stars indicate significance level: * $P < 0.05$, ** $P < 0.01$, *** $P < 0.001$. Cells were illuminated with 470 nm light at ~5 mW mm^{-2}.

Nature Methods: doi:10.1038/nmeth.1808

Supplementary Figure 11 ChETA$_A$ vs. ChIEF expression, cell health and photocurrent stability

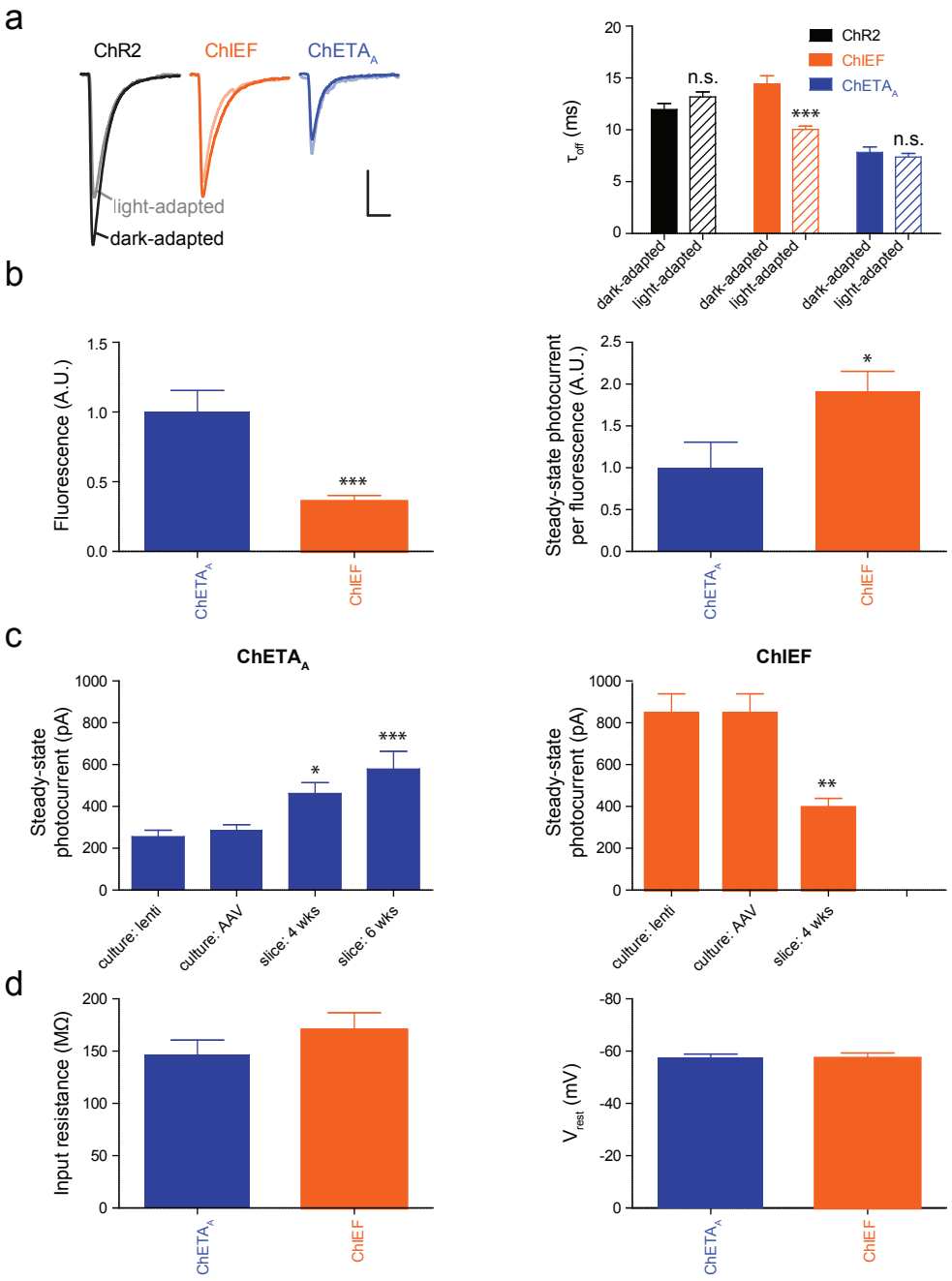

(**a**) Representative traces to demonstrate off-kinetics (τ_{off}) in response to 3 ms light pulses delivered in a dark-adapted condition vs. 3 ms light pulses following blue light-adaptation for ChR2 (*n* = 14), ChIEF (*n* = 12) and ChETA$_A$ (*n* = 10). 2nd pulse is indicated by the paler trace. Vertical and horizontal scale bars represent 200 pA and 20 ms, respectively. Summary graphs demonstrate the change in off-kinetics between a 1st light pulse (dark-adapted) and a 2nd light pulse (light-adapted). (**b**) ChETA$_A$ (*n* = 10) has significantly higher fluorescence intensity (in arbitrary units, A.U.) measured at the soma compared to ChIEF (*n* = 15, *P* < 0.001). However ChIEF has significantly higher steady-state photocurrent per unit fluorescence (*P* < 0.05, *n* = 6 and *n* = 13 for ChETA$_A$ and ChIEF, respectively). (**c**) Comparison of ChETA$_A$ and ChIEF expression across experimental preparations using steady-state photocurrent magnitude as a surrogate quantification of membrane expression. Note that only the 4 week expression time-point was examined for ChIEF. (**d**) Cell input resistance and resting membrane potential were similar for the two tools (*n* = 20 and *n* = 16 for ChETA$_A$ and ChIEF, respectively). All population data is plotted as mean ± s.e.m. Stars indicate significance level: * *P* < 0.05, ** *P* < 0.01, *** *P* < 0.001. Cells were illuminated with 470 nm light at ~5 mW mm^{-2}.

Supplementary Figure 12 ChETA$_A$ vs.ChIEF plateau potential, spiking performance and correlation with photocurrent

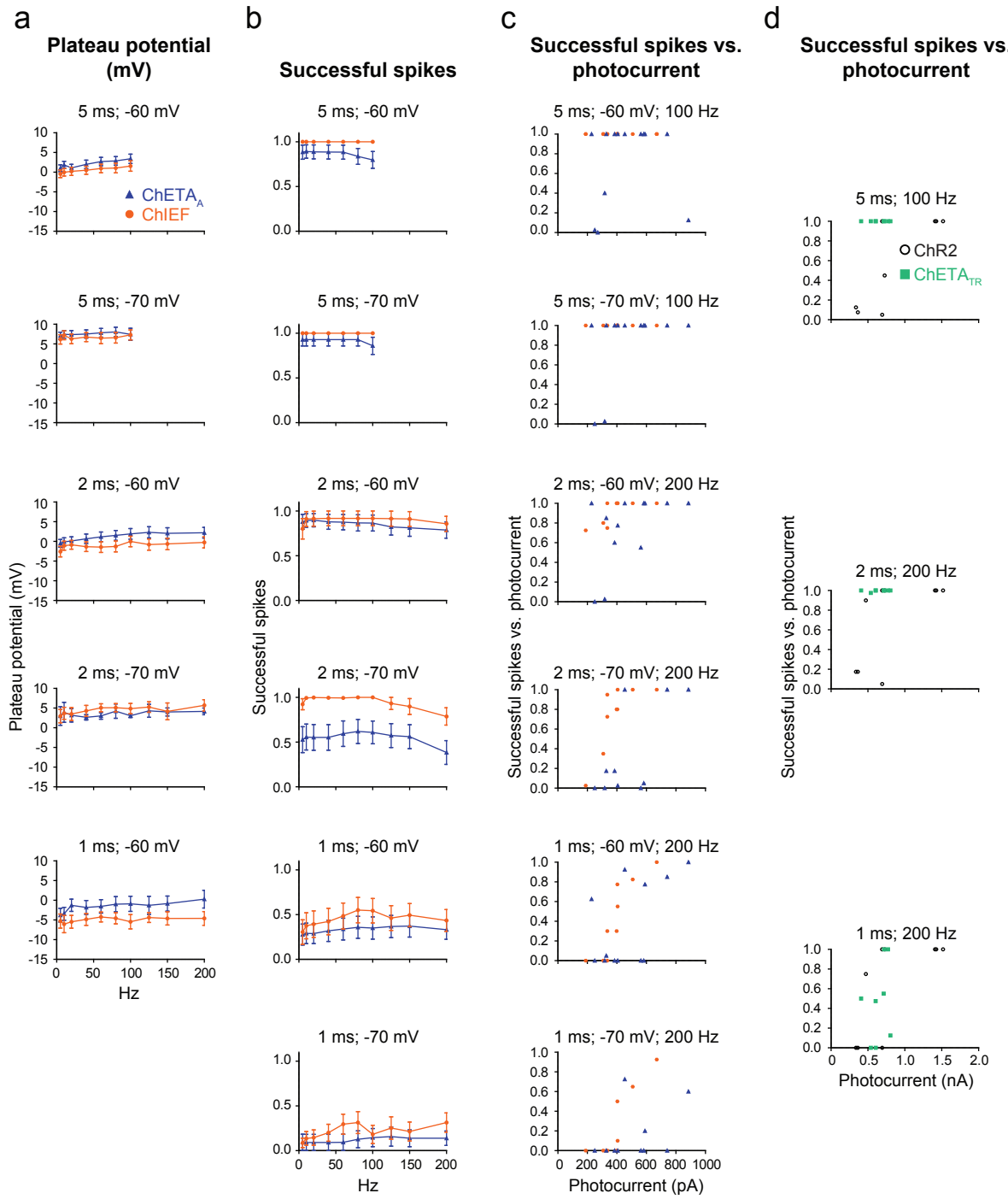

(**a**) Plateau potential vs. stimulation frequency (5-200 Hz for 1 and 2 ms pulse-width; 5-100 Hz for 5 ms pulse-width) across varying pulse-widths (5 ms, 2 ms, 1 ms) and holding potentials (-60 mV, -70 mV; *n* = 3-13 and *n* = 3-11 for ChETA$_A$ and ChIEF, respectively). The 1 ms/-70 mV condition is omitted due to insufficient number of cells with sufficient spiking to calculate plateau. (**b**) Proportion of successful spikes vs. stimulation frequency at varying pulse-widths (5 ms, 2 ms, 1 ms) and holding potentials (-60 mV, -70 mV; *n* = 11-18 and *n* = 11-12 for ChETA$_A$ and ChIEF, respectively). (**c**) Relationship between the proportion of successful spikes vs. steady-state photocurrent magnitude at varying pulse-widths (5 ms, 2 ms, 1 ms), and holding potentials (-60 mV, -70 mV; *n* = 10-12 and *n* = 9-14 for ChETA$_A$ and ChIEF, respectively). (**d**) For comparison, relationship between spiking performance and steady-state photocurrent for ChR2 (*n* = 8-9) and ChETA$_{TR}$ (*n* = 8) at varying pulse-widths (5 ms, 2 ms, 1 ms). All population data is plotted as mean ± s.e.m. Stars indicate significance level: * $P < 0.05$, ** $P < 0.01$, *** $P < 0.001$. Cells were illuminated with 470 nm light at ~5 mW mm^{-2}.

Supplementary Figure 13 ChETA$_A$ vs.ChIEF temporal stationarity, multiple spikes and correlation with photocurrent

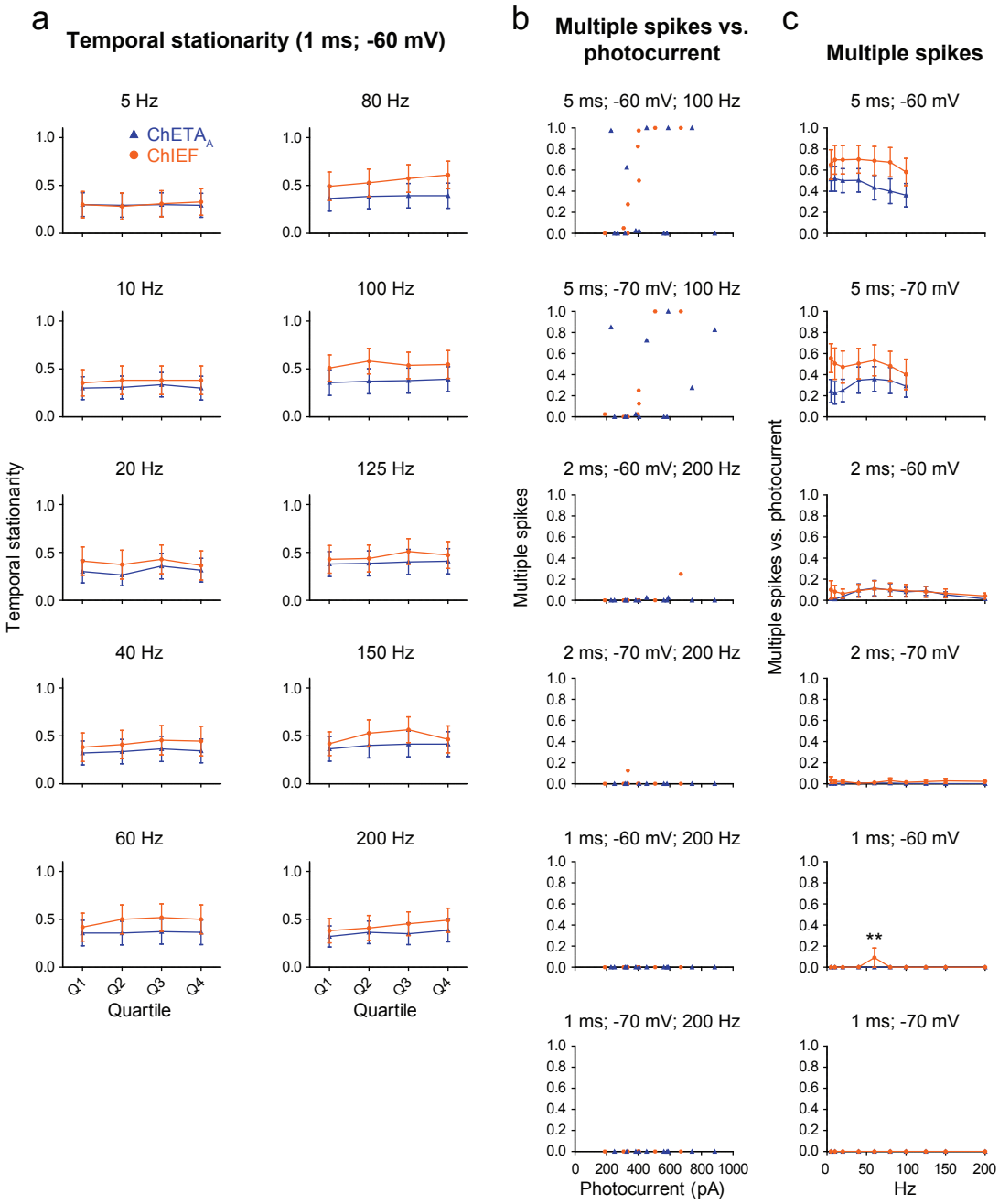

(**a**) Temporal stationarity over a range of stimulation frequencies (5-200 Hz), all at 1 ms pulse-width, -60 mV holding potential. The 40 pulses of the train are divided into quartiles and the proportion of successful spikes elicited in each quartile (out of 10) is quantified for ChETA$_A$ (*n* = 14) and ChIEF (*n* = 11). (**b**) Relationship between multiple spikes and steady-state photocurrent size at varying pulse-widths (5 ms, 2 ms, 1 ms), and holding potentials (-60 mV, -70 mV; *n* = 10-12 and *n* = 9-14 for ChETA$_A$ and ChIEF, respectively. (**c**) Proportion of multiple spikes vs. stimulation frequency at varying pulse-widths (5 ms, 2 ms, 1 ms) and holding potentials (-60 mV, -70 mV) for ChETA$_A$ (*n* = 11-18) and ChIEF (*n* = 11-12). All population data is plotted as mean ± s.e.m. Stars indicate significance level: * $P < 0.05$, ** $P < 0.01$, *** $P < 0.001$. Cells were illuminated with 470 nm light at ~5 mW mm^{-2}.

Nature Methods: doi:10.1038/nmeth.1808

Supplementary Figure 14 ChETA$_A$ vs.ChIEF spike latency and latency spread across a pulse train

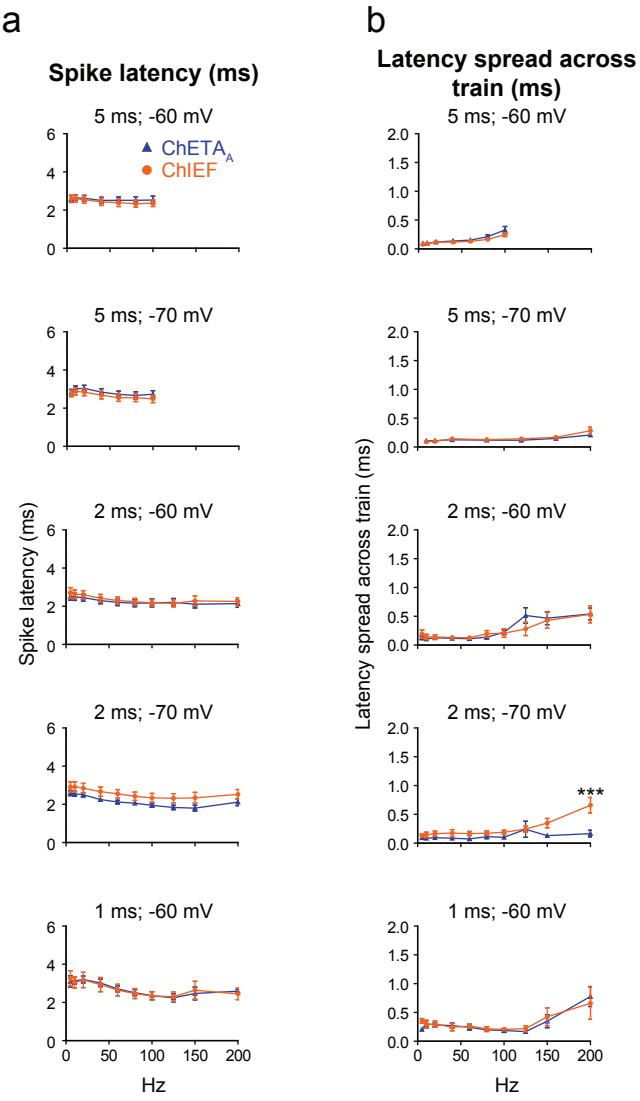

(**a**) Latency to spike vs. frequency (5-200 Hz for 1 and 2 ms pulse-width; 5-100 Hz for 5 ms pulse-width) at varying pulse-widths (5 ms, 2 ms, 1 ms) and holding potentials (-60 mV, -70 mV). Latency is approximately 3 ms for both ChETA$_A$ (*n* = 5-15) and ChIEF (*n* = 4-12) across conditions. The 1 ms/-70 mV condition is omitted due to insufficient number of cells with sufficient spiking to calculate latency. (**b**) Latency spread across train vs. frequency at varying pulse-widths (5 ms, 2 ms, 1 ms) and holding potentials (-60 mV, -70 mV; *n* = 5-15 and *n* = 4-12 for ChETA$_A$ and ChIEF, respectively). The 1 ms/-70 mV condition is omitted due to insufficient number of cells with sufficient spiking to calculate latency spread. All population data is plotted as mean ± s.e.m. Stars indicate significance level: * $P < 0.05$, ** $P < 0.01$, *** $P < 0.001$. Cells were illuminated with 470 nm light at ~5 mW mm^{-2}.

Nature Methods: doi:10.1038/nmeth.1808

Supplementary Figure 15 Hyperpolarizing tools: enhancement of membrane-trafficking and expression

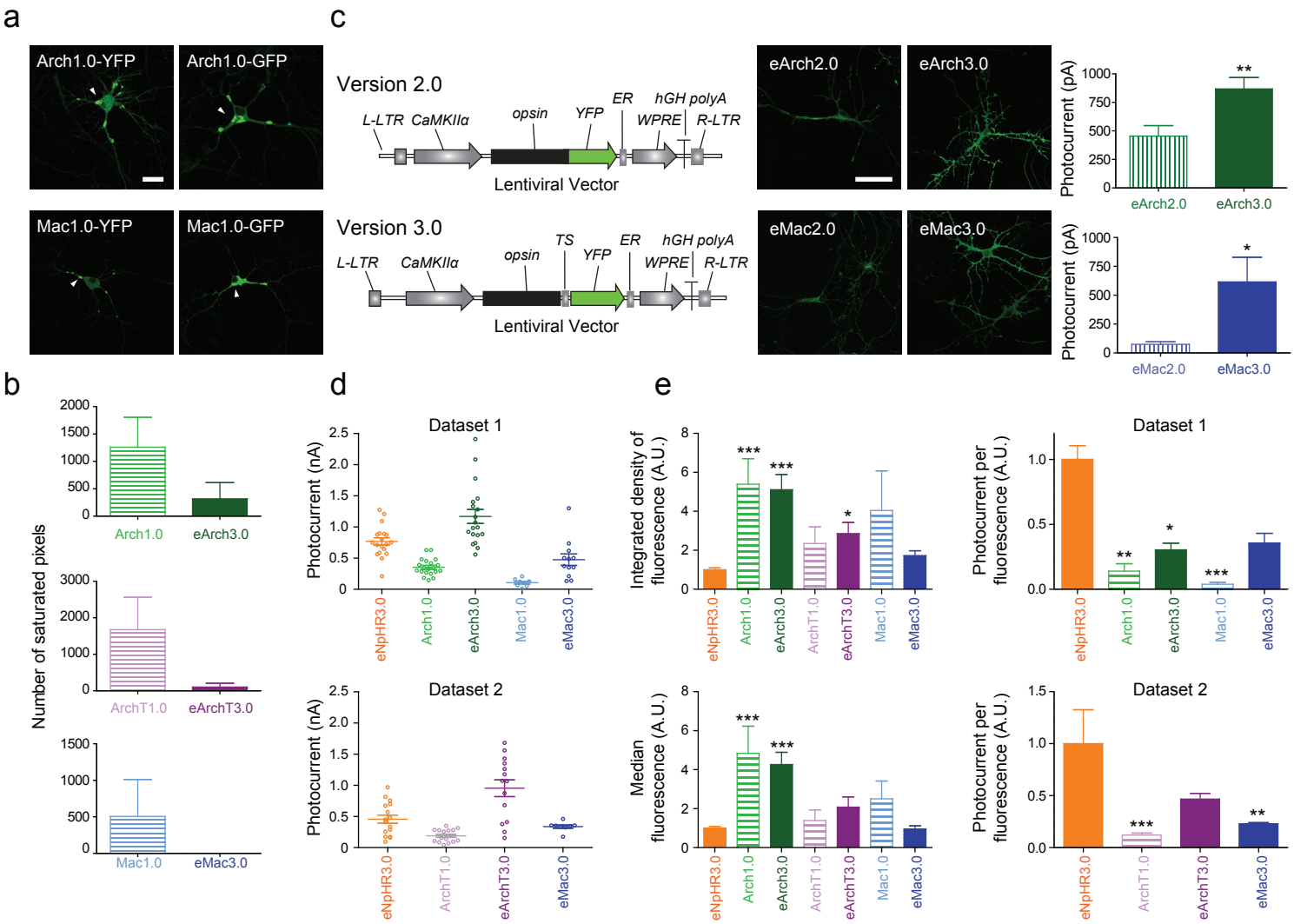

(**a**) Confocal images under matched conditions of cultured hippocampal pyramidal neurons expressing Arch1.0 and Mac1.0 fused to eYFP and GFP. White arrowheads indicate examples of abnormal aggregates. Scale bar represents 25 µm. (**b**) Number of saturated pixels on the fluorescence image is used as a surrogate quantification of the extent of protein aggregation in the cell (*n* = 3-12). All eNpHR3.0-expressing cells had 0 saturated pixels (data not shown). (**c**) Vector diagrams for 2.0 and 3.0 versions of hyperpolarizing opsins packaged in a lentiviral backbone: 2.0 constructs include an endoplasmic reticulum (ER) export sequence after the eYFP sequence and 3.0 constructs include an additional trafficking signal located between the opsin and the eYFP sequence. Confocal images under matched conditions of cultured hippocampal pyramidal neurons demonstrating enhanced membrane trafficking of eArch3.0 and eMac3.0 relative to 2.0 versions. Scale bar represents 50 µm. Summary graphs of 3.0 vs. 2.0 photocurrents (*n* = 7-15). (**d**) Spread of onset photocurrent magnitude around the mean value for datasets 1 and 2. These two datasets were not consolidated as the mean value for eNpHR3.0 photocurrents differed between the datasets. We therefore present the datasets separately, using eNpHR3.0 as a point of reference for each (*n* = 8-20 for Dataset 1 and 8-16 for Dataset 2). (**e**) Quantification of membrane expression: Integrated fluorescence density and median fluorescence (in arbitrary units A.U.) over a defined region of interest (ROI) of a cell. Arch1.0 and eArch3.0 have significantly greater integrated fluorescence density and median fluorescence relative to eNpHR3.0 ($P < 0.01$, n = 3-28). However, eNpHR3.0 has the largest photocurrent magnitude per unit of integrated fluorescence (*n* = 3-18 for Dataset 1 and 7-10 for Dataset 2). All population data is plotted as mean ± s.e.m. Stars indicate significance level: * $P < 0.05$, ** $P < 0.01$, *** $P < 0.001$. Unless otherwise indicated, eNpHR3.0 was activated at 590 nm light, while all others were activated with 560 nm light, at ~5 mW mm^{-2}.

Nature Methods: doi:10.1038/nmeth.1808

Supplementary Figure 16 Properties of hyperpolarizing optogenetic tools

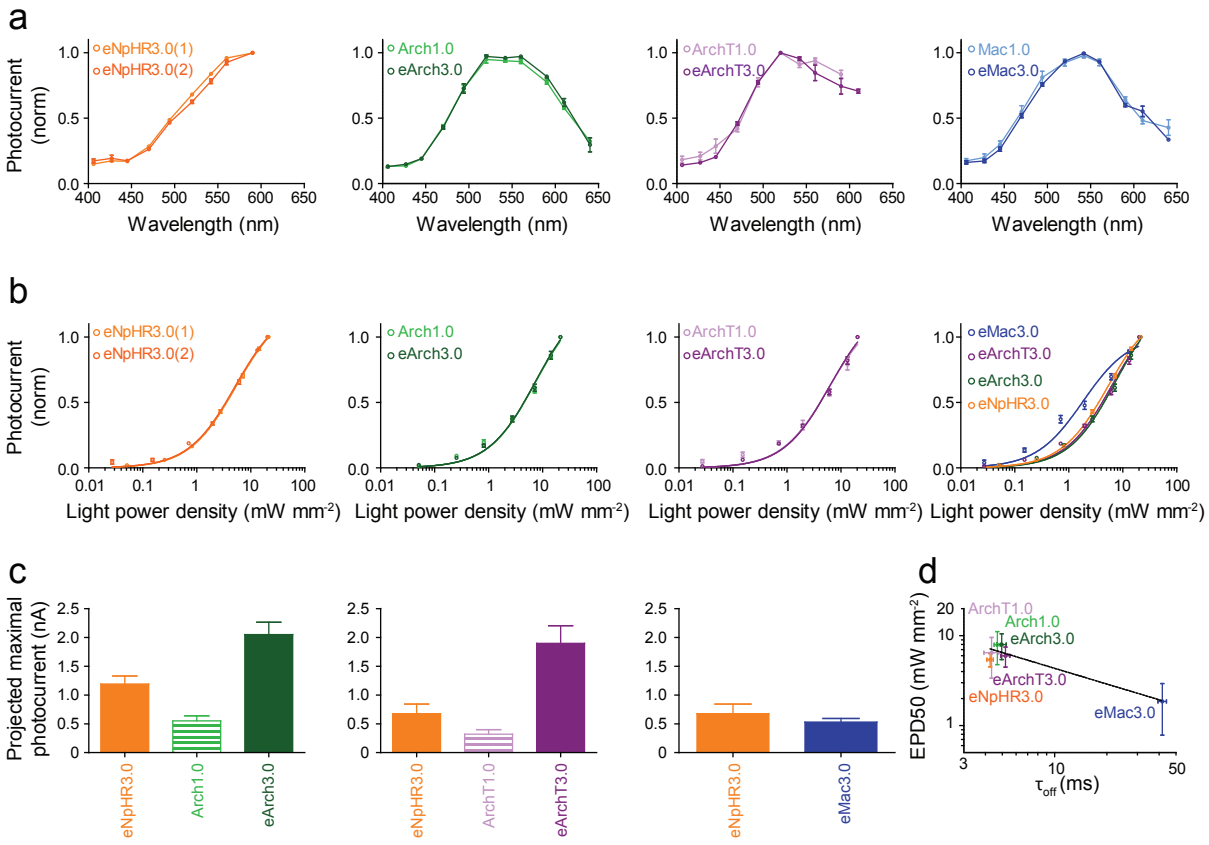

(**a**) Action spectra (photocurrent normalized to peak) for hyperpolarizing optogenetic tools. eNpHR3.0 datasets 1 and 2 have the same action spectra (*n* = 10), and all 1.0 vs. 3.0 comparisons are likewise consistent (*n* = 6-14). (**b**) EPD50 curves for inhibitory tools: Plots of normalized photocurrent magnitude vs. light power used to calculate EPD50 (light power density at which 50% of the maximum photocurrent magnitude is achieved) for the hyperpolarizing tools. eNpHR3.0 datasets 1 and dataset 2 have similar curves (*n* = 5-9), and all 1.0 vs. 3.0 comparisons are likewise consistent (*n* = 5-14). Comparison of EPD50 curves for all 3.0 hyperpolarizing tools: note that eMac3.0 has a left-shifted EPD50 curve compared to the other tools, indicating a lower EPD50 (*n* = 5-14). R^2 = 0.47 to 0.88. (**c**) Projected maximal photocurrents were determined from the non-linear fit of raw photocurrent vs. light power density (*n* = 5-10). (**d**) Relationship between EPD50 and off-kinetics (τ_{off}) for hyperpolarizing tools. The black line represents the best-fit regression, R^2 = 0.79. All population data is plotted as mean ± s.e.m. Stars indicate significance level: * $P < 0.05$, ** $P < 0.01$, *** $P < 0.001$. Unless otherwise indicated, eNpHR3.0 was activated at 590 nm light, while all others were activated with 560 nm light, at ~5 mW mm^{-2}.

Supplementary Figure 17 Hyperpolarizing tool performance with prolonged stimulation

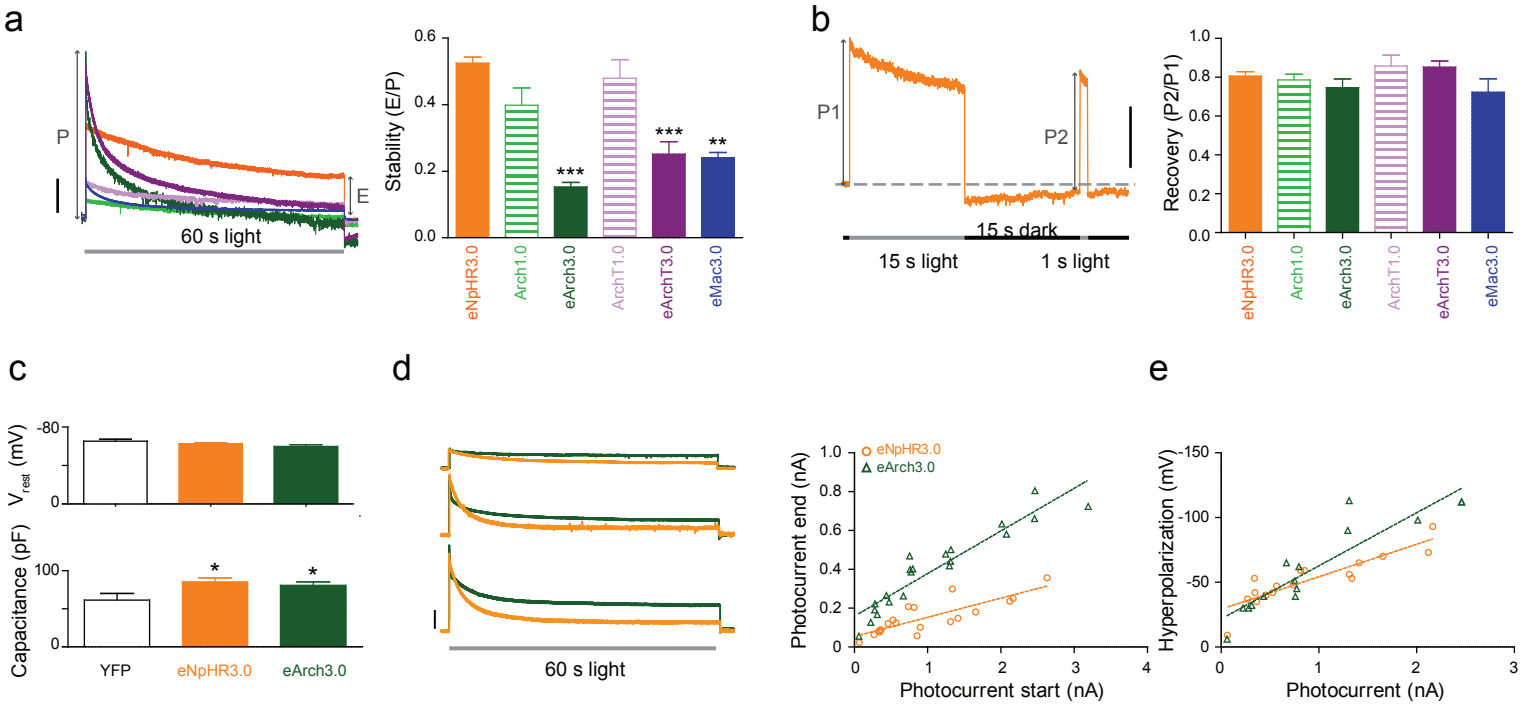

(**a**) Photocurrent stability across prolonged (60 s) light pulse in cultured neurons. Representative traces illustrate the decay in peak photocurrent over time. "P" and "E" illustrate the measurement of "peak" and "end" photocurrent magnitudes respectively, used to calculate photocurrent stability (ratio E/P). Vertical scale bar represents 250 pA. *n* = 5-17. (**b**) Representative trace and summary graph showing recovery (P2/P1 ratio) of photocurrent after prolonged light exposure (15 s) followed by 15 s darkness in cultured neurons. Vertical scale bar represents 250 pA. *n* = 5-17. (**c**) Cell health measures in slice for eNpHR3.0 and eArch3.0 compared with eYFP-expressing controls. *n* = 10-22. (**d**) Relationship between photocurrent magnitude at the start vs. end of a 60 s light pulse for eArch3.0 and eNpHR3.0 tested in slice. Photocurrent-matched representative traces for eArch3.0 (green, *n* = 21) and eNpHR3.0 (yellow, *n* = 19) in response to 1 s 560 nm continuous light pulse. Cells were illuminated with variable power densities to achieve approximately matched photocurrent magnitudes. Vertical scale bar represents 400 pA. Summary plot: lines represent regression fits. (**e**) Relationship between photocurrent (measured at -70 mV) and hyperpolarization magnitude. Lines represent regression fits. All population data is plotted as mean ± s.e.m. Stars indicate significance level: * $P < 0.05$, ** $P < 0.01$, *** $P < 0.001$. eNpHR3.0 was activated 590 nm light, while all others were activated with 560 nm light, at ~5 mW mm^{-2} unless otherwise indicated.

Nature Methods: doi:10.1038/nmeth.1808

Supplementary Table 1 Naming convention for depolarizing optogenetic tools

Name	Backbone	Mutation(s)
ChR2	ChR2	none
$ChR2_R$	ChR2	H134R
$ChETA_A$	ChR2	E123A
$ChETA_{AR}$	ChR2	E123A/H134R
$ChETA_T$	ChR2	E123T
$ChETA_{TR}$	ChR2	E123T/H134R
TC	ChR2	T159C
$ChETA_{TC}$	ChR2	E123T/T159C
CatCh	ChR2	L132C
ChIEF	ChR1/ChR2(1)	I170V
FR	ChR1/ChR2(2)	none
GR	ChR1/ChR2(3)	none
$C1V1_T$	ChR1/VChR1	E162T
$C1V1_{TT}$	ChR1/VChR1	E122T/E162T

Nature Methods: doi:10.1038/nmeth.1808

Supplementary Table 2 Cloning and mutagenesis primers

	gene	Restriction Site	Sequence
Opsin forward primers	hChR2	BamHI	gggggatccccgggtaccggtgccaccatggactatggcggcgctttg
	NpHR 1.0 & 3.0	BamHI	gcgggggatccccgggtaccggtaggccaccatgacagagaccctgcctcc
	NpHR 2.0	BamHI	gggggatccccgggtaccggtgccaccatgaggggtacgcccctgctcctcgtcgtctctctgttctctctgcttcaggacacagagaccctgcctcccg
	C1 (A-B) for FR	BamHI	gggggatccccgggtaccggtgccaccatgtcgcggaggccatggcttc
	FR	BamHI	C1 (A-B) for FR
	C1 (A-E) for GR	BamHI	gggggatccccgggtaccggtgccaccatgtcgcggaggccatggcttc
	GR	BamHI	C1 (A-E) for GR
	Arch	BamHI	ccggatccgccaccatggaccccatcgctctgcaggc
	ArchT	BamHI	ccggatccccgggtaccggtaggccaccatggacccaattgcactgcag
	Mac	BamHI	gggggatccgccaccatgatcgtggaccagttcg
	C1 for C1V1	BamHI	cgggggatccccgggtaccggtaggccaccatgtcgcggaggccatggc
	C1V1	BamHI	C1 for C1V1
Opsin reverse primers	hChR2	NotI	cggcggccgctggcacggctccggcctcggc
	NpHR 1.0 & 3.0	NotI	ggcggccgcatcatcagccggggtcccagaag
	NpHR 2.0	NotI	ggcggccgcatcatcagccggggtcccagaag
	C1-AB (for FR)	N/A	gaatgaccgggcaggtgagcagccactccgcgtaacgaag
	FR	NotI	gtggcggccgccttgccggtgcccttgttgac
	C1-AE for GR	N/A	cccttctggccccaagaggaacaggatggggaacatac
	GR	NotI	ggtggcggccgccttgccggtgcccttgttg
	Arch	NotI	cttggcggccgccttgctcactgctactaccggtcggtcggcgg
	ArchT	NotI	ggtggcggccgcaggctccggggcttccgtatcc
	Mac	NotI	ggcggccgccttgctcactgctactaccggtcgggcg
	C1 for C1V1	N/A	cagaaggaccgggcaggtgagcagccactccgcgtaacgaagc
	C1V1	NotI	cggcggccgcgtcctcctcttcagccaccag
YFP forward primers	eYFP	NotI	gcggccgccgtgagcaagggcgaggagctg
	eYFP for 3.0	NotI	gatgcggccgccaagagcaggatcaccagcgagggcgagtacatccccctggaccagatcgacatcaacgtggtgagcaagggcgaggagctg
	eYFP for ChIEF	EcoRI	gcgaattcatggtgagcaagggcgaggag
YFP reverse primers	eYFP	EcoRI	ccgaattcttacttgtacagctcgtcc
	eYFP for 2.0 and 3.0	EcoRI	ccgaattctcattacacctcgttctcgtagcagaacttgtacagctcgtccatgccgagag
	eYFP for ChIEF	BsrGI	ctattacttgtacagctcgtccatg
Mutagenesis	ChR2 (E123A)	N/A	gcagtggctgcgctatgcagcctggctgctcacttgtcc
	ChR2 (E123T)	N/A	gcagtggctgcgctatgcaacctggctgctcacttgtcc
	ChR2 (L132C)	N/A	cacttgtcctgtcatctgtatccacctgagcaacc
	ChR2 (H132R)	N/A	gtcctgtcatccttatccgcctgagcaacctcaccggcc
	ChR2 (T159C)	N/A	gtctcagacatcgggtgtatcgtgtgggggc
	C1V1 (E122T)	N/A	ctacttgcggctgggagaccatttacgtggccacgatcg
	C1V1 (E162T)	N/A	ccgtgtggcttcgttacgcgacctggctgctcacctgccc